Nanoscale

Accepted Manuscript

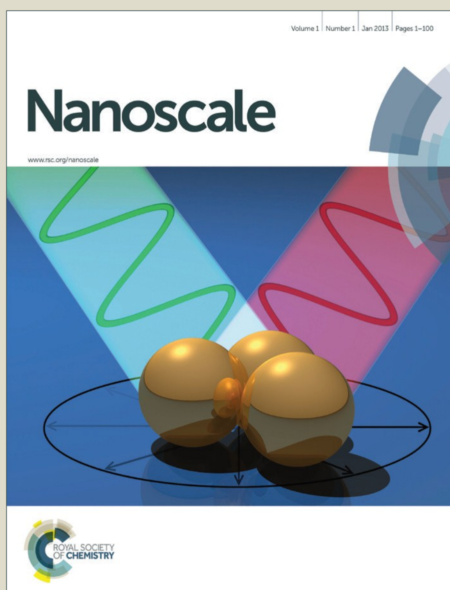

This is an *Accepted Manuscript*, which has been through the Royal Society of Chemistry peer review process and has been accepted for publication.

Accepted Manuscripts are published online shortly after acceptance, before technical editing, formatting and proof reading. Using this free service, authors can make their results available to the community, in citable form, before we publish the edited article. We will replace this *Accepted Manuscript* with the edited and formatted *Advance Article* as soon as it is available.

You can find more information about *Accepted Manuscripts* in the Information for Authors.

Please note that technical editing may introduce minor changes to the text and/or graphics, which may alter content. The journal's standard Terms & Conditions and the Ethical guidelines still apply. In no event shall the Royal Society of Chemistry be held responsible for any errors or omissions in this *Accepted Manuscript* or any consequences arising from the use of any information it contains.

ROYAL SOCIETY OF CHEMISTRY

www.rsc.org/nanoscale

Please do not adjust margins

Nanoscale

ARTICLE

Fast and Large-Area Growth of Uniform MoS_2 Monolayers on Molybdenum Foils

Received 00th January 20xx,
Accepted 00th January 20xx

DOI: 10.1039/x0xx00000x

www.rsc.org/

Guoan Tai,[a] Tian Zeng,[a,b] Jin Yu,[a] Jianxin Zhou,[a] Yuncheng You,[a,b] Xufeng Wang,[a,b] Hongrong Wu,[a] Xu Sun,[a] Tingsong Hu[a,b] and Wanlin Guo[a]

Controllable synthesis of two-dimensional crystal monolayers in a large area is a prerequisite for potential applications, but growth of transition metal dichalcogneides monolayers in a large area with spatial homogeneity remains a great challenge. Here we report a novel and efficient method to fabricate large-scale MoS_2 monolayers by direct sulfurization of pre-annealed molybdenum foil surfaces with large grain boundaries of more than 50 μm in size at elevated temperature. Continuous MoS_2 monolayers can be formed uniformly by sulfurizing the Mo foils in sulfur vapor at 600 °C within 1 min. At lower temperature even down to 500 °C, uniform MoS_2 monolayers can still be obtained but in a much longer sulfurizing duration. It is demonstrated that the formed monolayers can be nondestructively transferred onto arbitrary substrates by removing the Mo foil using diluted ferric chloride solution and can be successfully fabricated into photodetectors. The results show a novel avenue to efficiently fabricate two-dimensional crystals in a large area in a highly controllable way and should have great potential for the development of large-scale applications of the two-dimensional crystals in electrophotonic systems.

1. Introduction

Two-dimensional (2D) atomic-layered materials have attracted a great deal of attention in the past decade because of their exceptional electronic, optical, magnetic, mechanical and thermal properties.[1-10] Although graphene is by far the most studied 2D crystal, the lack of a bandgap impedes its applications in semiconducting and photonic devices.[3-5] Consequently, considerable attention has shifted towards 2D layered transition-metal dichalcogenides (TMDs).[6-19] Among all the TMD materials, three-atom-thick molybdenum disulphide (MoS_2) has attracted extensive interest because monolayer MoS_2 is a direct band gap semiconductor with a band gap of 1.8-2.0 eV due to quantum confinement effect; while bulk MoS_2 is indirect bandgap (1.2 eV).[20,21] Monolayer MoS_2 has rich physical properties, including switching characteristic, superconductivity and fascinating valley-dependent photoluminescence.[22-24] Therefore, it has attracted wide interest in field effect transistors, logic circuits, photodetectors, light emitters and valleytronics.[22,25-29]

Controllable synthesis of large-scale and uniform monolayer MoS_2 is a prerequisite for fulfilling the application potentials. The simple exfoliation of MoS_2 could not satisfy the size and scale requirements. Thus, chemical vapor deposition (CVD) methods, such as decomposition of thiomolybdates, and sulfurization of Mo films or molybdenum compounds (such as MoO_3 and $MoCl_5$), have been developed to obtain MoS_2 monolayers on diverse substrates such as SiO_2/Si, sapphire, strontium titanate, mica and graphene.[30-41] However, two-source (sulfur and MoO_3 or $MoCl_5$) CVD methods had been employed to obtain MoS_2 monolayers with triangular islands in size of tens of micrometers,[34-39] and the most used SiO_2 substrates usually result in the random orientation of the MoS_2 domains. To address this problem, some layered materials such as nearly lattice-matched mica and graphene was used as the growth substrates,[40,41] while the as-prepared MoS_2 grains still showed a random orientation. On the other hand, transferring the MoS_2 monolayers formed onto these substrates for further device fabrication was usually undergone with strongly corrosive hydrogen fluoride (HF) or strong alkali, which may destruct the MoS_2 lattice and pollute the environment. Thus it is extremely important to develop a green and low-cost technique to prepare continuous, uniform MoS_2 monolayers for industrial scale applications.

In this article, we report an easy and fast method for the growth of uniform MoS_2 monolayers of the order of centimeters by directly sulfurizing the Mo foil surfaces in sulfur (S) vapor at 600 °C within 1 min. In contrast to conventional exfoliation or other CVD methods, the present route toward the MoS_2 monolayers is very straightforward: only one element, S, is deposited on pre-annealed Mo foils. The obtained films are continuous and uniform MoS_2 monolayers, and are easily transferrable to various substrates by removing the Mo foil using diluted ferric chloride ($FeCl_3$) solution. We also fabricated a vertical p-n junction photodetector composed

[a] The State Key Laboratory of Mechanics and Control of Mechanical Structures, Key Laboratory for Intelligent Nano Materials and Devices of Ministry of Education and Institute of Nanoscience, College of Aerospace Engineering, Nanjing University of Aeronautics and Astronautics, Nanjing 210016, China. E-mail: taiguoan@nuaa.edu.cn, wlguo@nuaa.edu.cn
[b] School of Material Science and Technology, Nanjing University of Aeronautics and Astronautics, Nanjing 210016, China.
†Electronic Supplementary Information (ESI) available: Optical images, XPS spectra and UV-vis absorbance spectrum of the samples. See DOI: 10.1039/x0xx00000x

Nanoscale Accepted Manuscript

Please do not adjust margins

Please do not adjust margins

of the monolayer MoS_2 and p-type silicon to demonstrate its photoresponse property. This work paves the way for large-scale applications of the 2D MoS_2 in electronic and photonic devices.

2. Experimental

2.1 Growth and transfer of monolayer MoS_2

Typically, the molybdenum foil (20 µm, Shengyuan, 99.95%) with length of 80 mm and width of 30 mm was cleaned and degreased by ethanol, acetone, and IPA, respectively, and then polished by concentrated sulfuric acid at room temperature for 5 min under ultrasonic, consequently annealed at 1400 °C for 10 h under 50 sccm H_2 atmosphere which induced recrystallization. After that, the MoS_2 monolayers were prepared by a CVD procedure at the atmospheric pressure using ultrahigh-purity argon as the carrier gas. A crucible containing 500 mg of sulfur (≥99.5% purity, Alfa Aesar) was located upstream from the Mo foils; this zone was heated to a temperature of 150 °C with a high-temperature ceramic heating ring. The detailed growth process is as follows: set the temperature of 300 °C with 100 sccm for 10 min, ramp to 600 °C with a rate of 30 °C min^{-1} and 10 sccm of carrier gas flow, set the temperature to 600 °C for 1 min, cool down to 550 °C with 100 sccm gas flow, and then open the furnace for rapid cooling.

MoS_2 layer at one-side of the Mo foil was removed by mechanical grinding on SiC papers up to #1200 grit size. The protective layer PMMA was initially spin-coated onto one side of the as-prepared sample. The sacrificed Mo foil can be dissolved after dipping into 2 M iron chloride. Then, the MoS_2 coated PMMA was transferred onto SiO_2/Si substrate and the PMMA layer was removed using hot acetone at 80 °C for 1 h. They could also be easily transferred onto extensive substrates such as 285 nm SiO_2/Si, quartz, PET, PEN and glass.

2.2 Structural characterization of monolayer MoS_2

The morphology of the MoS_2 films was examined by optical microscopy (Olympus BX41). Transmission electron microscopy (TEM) images and selected area electron diffraction (SAED) patterns were performed on a FEI Tecnai G20 system. Field emission scanning electron microscopy (FESEM) images were obtained on a FEI Sirion 200. The thickness profile of as-prepared MoS_2 films was measured by atomic force microscopy (AFM, DI Nanocope 8). Raman spectroscopy was carried out using a Horiba Jobin Yvon LabRAM HR-Evolution Raman microscope with an excitation laser of 514 nm and an estimated laser spot size of 2 µm. Elemental composition analysis was performed using X-ray photoelectron spectroscopy (ESCALAB 250, Thermo Fisher Scientific Inc.) with focused monochromatized Al Ka radiation. Room temperature PL was measured on a LabRAM HR800 micro-Raman spectrometer with 532 nm excitation light.

2.3 Fabrication and measurement of MoS_2 devices

To fabricate the MoS_2/p-Si heterojunction photodetector, we used p-type Si wafers with a resistivity of 0.1-0.5 Ωcm which corresponds to a boron doping level between 3×10^{16}-10^{17} cm^{-3}. The preparation process of the Si devices was as follows: first, the wafers were first cut into smaller pieces with the size of 1 cm ×1 cm; secondly, the SiO_2 layer on the Si was completely etched by immersing it in 5% diluted hydrofluoric acid (HF) for 2 min; then, a photosensitive area of 0.2 × 0.2 cm^2 PDs was defined by a blue tape; fourthly, 300 nm SiO_2 was deposited on the p-Si wafers by a sputtering process; Finally, a layer of Ti/Au with a total thickness of 150 nm was deposited on the 300 nm SiO_2 to construct a square electrode. Consequently, MoS_2 monolayers were transferred onto the Si device and then the MoS_2-Si photodetector was heated at 150 °C for 30 min in vacuum. In the photodetector, the Au thin film, contacted with the MoS_2 film, acts as a negative electrode, and indium dots contacted with the p-Si paste acts as a positive electrode. Current-voltage characteristics of devices were measured by a Keithley 2400 sourcemeter under dark and illuminated conditions. We used a commercial green LED with a wavelength of 525 nm as the illuminated light. All the measurements were performed at room temperature.

2.4 Theoretical calculation

To study the formation mechanism of MoS_2 on Mo (100) and Mo (111), we performed first principles calculations on the structure and binding of S atoms on Mo surfaces. All the results presented in our work were carried out by using Vienna ab initio simulation package (VASP). The generalized gradient approximation (GGA) with Perdew-Burke-Ernzerhof (PBE) exchange-correlation functional was adopted. The projector augmented wave potentials were used with a kinetic energy cutoff of 350 eV, and Brillouin zone integration was sampled by a 15×15 k mesh. Seven-layer slabs of Mo (100) and Mo (111) were chosen to study the surface properties of Mo with the bottom two atom layers fixed and the rest as buffer layers. The system was simulated with a periodic boundary condition by placing S atom on the surface of a 1×1 (1 ML), 2×1 (0.5 ML) and 2×2 (0.25 ML) unit cell of Mo slabs, spaced by 25 Å along the normal direction. The geometry was fully relaxed until the force on each atom was less than 0.01 eV/Å. The binding energy for S atom adsorbed on Mo slabs was calculated using $E_{bind}=E_{system}-E_{Mo}-E_X$, where E_{system}, E_{Mo} and E_X are the energies of the adsorbed system, Mo slabs and S atom, respectively.

3. Results and discussion

3.1 Synthesis and characterization of MoS_2 monolayer

Growth and transfer of MoS_2 monolayers grown on molybdenum foils are schematically demonstrated (Fig. 1a and b). First, the molybdenum (Mo) foils were annealed in 1400 °C for 10 h under high-purity H_2 atmosphere to smooth the surface of the foils and enlarge the grain boundaries (Fig. S1a-c, ESI†). X-ray diffraction (XRD) diffraction peaks were indexed to the cubic (fcc) phase of Mo foil (space group: $Fm\bar{3}m$) with lattice constants of 0.315 nm (JCPDS card: 89-5023), and two strong peaks showed that the annealed Mo foil had high crystallinity (Fig. S1d, ESI†). Then, the foil surfaces were sulfurized by sulfur vapor, and the MoS_2 monolayers were controllably grown on the Mo foils at 600 °C for 1 min. In contrast, the continuous monolayers were grown on the Mo foils at 500 °C for over 60 min. Finally, the monolayers were successfully transferred onto diverse substrates for further characterization and device application.

Nanoscale Accepted Manuscript

This journal is © The Royal Society of Chemistry 20xx

Please do not adjust margins

Please do not adjust margins

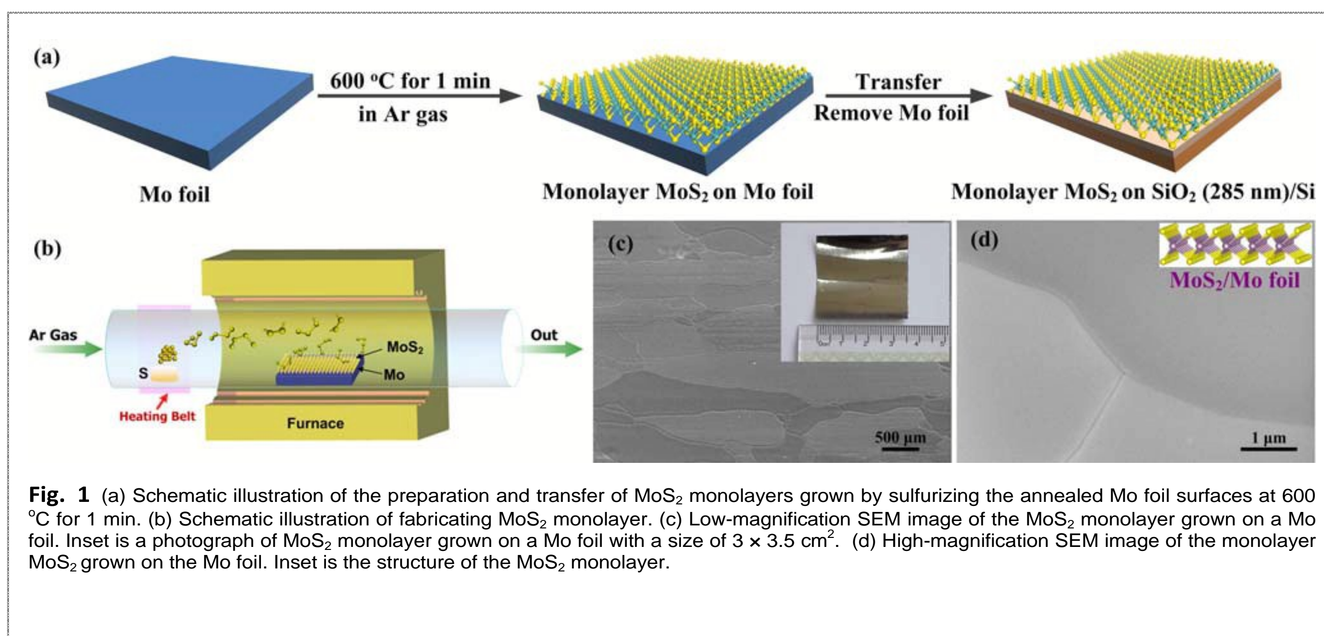

Fig. 1 (a) Schematic illustration of the preparation and transfer of MoS_2 monolayers grown by sulfurizing the annealed Mo foil surfaces at 600 °C for 1 min. (b) Schematic illustration of fabricating MoS_2 monolayer. (c) Low-magnification SEM image of the MoS_2 monolayer grown on a Mo foil. Inset is a photograph of MoS_2 monolayer grown on a Mo foil with a size of 3 × 3.5 cm^2. (d) High-magnification SEM image of the monolayer MoS_2 grown on the Mo foil. Inset is the structure of the MoS_2 monolayer.

Scanning electron microscopy (SEM) was used to characterize the structure of the obtained MoS_2 monolayer. The result showed that a nearly atomically smooth MoS_2 monolayer was formed on the surface of the Mo foil, and their structures with large grain boundaries of more than 50 µm in size which is in good agreement with those before the sulfurization (Fig. 1c and d, and Fig. S1b and c, ESI†). The optical contrast between the MoS_2 monolayer and the 285 nm SiO_2/Si substrate showed that the film was uniform in a large area (Fig. 2a). Atomic force microscopy (AFM) image showed that the thickness of the MoS_2 film was around 0.85 nm, which confirmed that the film was monolayer (Fig. 2b).[42]

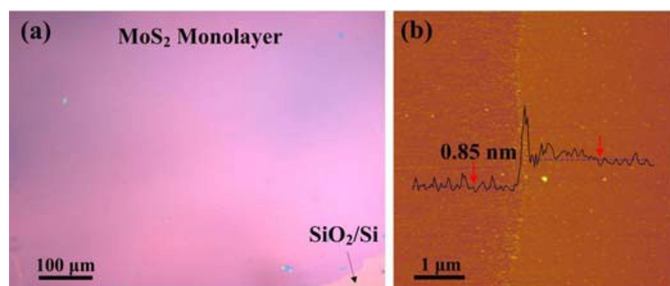

Fig. 2 (a) Optical image of as-grown MoS_2 monolayers transferred onto a 285 nm SiO_2/Si substrate. (b) AFM topographical image of the MoS_2 monolayer transferred onto the 285 nm SiO_2/Si substrate. Height profile along the red line in the inset shows a thickness of 0.85 nm, indicating that the film is indeed monolayer.

Scanning electron microscopy (SEM) and transmission electron microscope (TEM) were employed to confirm the quality of the MoS_2 monolayer prepared by the direct sulfurization. SEM image showed that the MoS_2 monolayer transferred onto 285 nm SiO_2/Si substrate was uniform and continuous (Fig. 3a). TEM image showed that an atomic MoS_2 layer was covered onto the holes of the TEM grid and the layer with a rolled-up edge occurred in some regions (Fig. 3b). A typical TEM image of the thin film with a folded edge was shown in the upper right side of Fig. 3b, further confirming that the film is indeed monolayer. Fig. 3c showed that the MoS_2 atomic layer was uniform and continuous. High magnification TEM image in Fig. 3d and the corresponding selected-area electron diffraction (SAED) pattern in the inset showed that the film exhibited high crystallinity. A high-resolution TEM (HRTEM) image revealed the 2H hexagonal lattice structure of the monolayer MoS_2, as shown in Fig. 3e. To clearly index the lattice directions, the corresponding atomic layer of MoS_2 was reconstructed by masking the fast Fourier transform (FFT) pattern (in the inset of Fig. 3f), and the result indicated the 2H hexagonal lattice structure of MoS_2 with lattice spacings of ~2.87 and ~1.68 Å , corresponding to (100) and (110) planes, respectively.

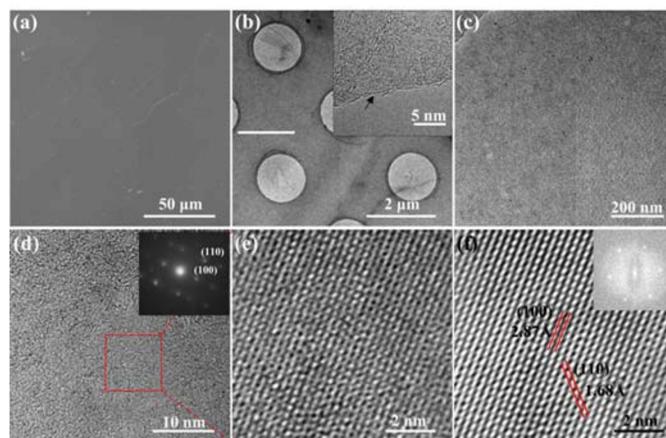

Fig. 3 (a) Field-emission SEM image of MoS_2 monolayer transferred onto a 285 nm SiO_2/Si substrate. (b) Low-magnification TEM image of MoS_2 monolayer covering a TEM grid. Inset is a typical TEM image of a folded edge and the black arrow shows that the film is of monolayer thickness. (c) TEM image of the MoS_2 monolayer over a hole of the TEM grid. (d) Enlarged TEM image of the MoS_2 monolayer. Inset is the corresponding SAED pattern. (e) High-resolution TEM (HRTEM) image taken from the region indicated by the red region in (d). (f) Reconstructed HRTEM image by masking the fast Fourier transform (FFT) pattern, indicating clearly that the structure of the thin film has a 2H MoS_2

Nanoscale Accepted Manuscript

This journal is © The Royal Society of Chemistry 20xx

Please do not adjust margins

Please do not adjust margins

character. The lattice spacings of 2.87 and 1.68 A can be indexed into the (100) and (110) crystal faces of 2H MoS_2.

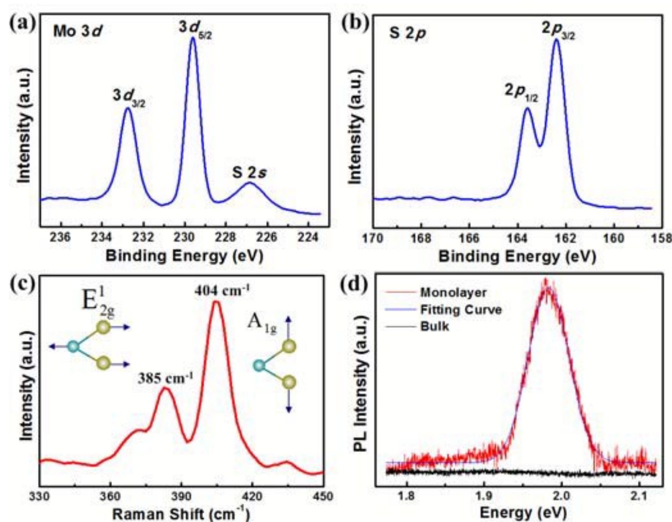

Fig. 4 (a) XPS spectrum of Mo 3d and S 2s peaks. (b) XPS spectrum of S 2p peaks. (c) Raman spectrum of the as-grown MoS_2 monolayer, normalized to the peak intensity of silicon. (d) A comparison of photoluminescence spectra taken from the monolayer and the bulk MoS_2. The blue line indicates a fitting of the PL peak of the monolayer, corresponding to an energy of 1.98 eV.

The X-ray photoelectron spectroscopy (XPS) was used to investigate the chemical states of Mo and S in the sample (Fig. 4a and b). The high-resolution XPS spectra showed that the binding energies of Mo $3d_{3/2}$ and Mo $3d_{5/2}$ were located at 232.8 and 229.6 eV, respectively, which could be attributed to Mo^{4+} in MoS_2 (Fig. 4a). The absence of a peak at around 235.8 eV indexed to Mo^{6+} $3d^{5/2}$ of MoO_3 indicated that the oxidation of Mo was negligible. The binding energies at 162.4 and 163.6 eV in the S 2p spectrum were characteristic of the S^{2-} of MoS_2 (Fig. 4b).[43] From the XPS spectra, the sulphur-to-molybdenum stoichiometric ratio (S:Mo), as estimated from the respective integrated peak area of XPS spectra, was close to 1.87.

The MoS_2 monolayer was also further confirmed by Raman spectroscopy in Fig. 4c. Raman spectrum of the monolayer showed that the two intense peaks at 385 and 404 cm^{-1} are $E_{2g}{}^1$ and A_{1g} modes of MoS_2.[44] The $E_{2g}{}^1$ and A_{1g} modes can be assigned to in-plane vibration of two S atoms with respect to the Mo atom and out-of-plane vibration of S atoms, respectively. The frequency difference of the two modes is around 19 cm^{-1}, which is consistent with the reported frequency difference of monolayer MoS_2 from 19 to 20 cm^{-1}.[45,46] Moreover, Raman spectra of the sample in arbitrary four regions were measured to verify the uniformity of the obtained MoS_2 monolayers (Fig. S2, ESI†).

The absorption spectrum of the MoS_2 monolayer was measured on a quartz substrate (Fig. S3, ESI†). The two characteristic absorption peaks were located at 598 nm (2.08 eV) and 651 nm (1.91 eV), respectively, which resulted from direct transition from the valance to conduction band at the *K*-point of the Brillouin zone, known as the B and A transitions.[24,47-49] The two peaks with little energy difference can be attributed to the spin–orbital splitting of the valence band.[24,49] In addition, the broad absorption band at 414 nm (3.0 eV) was also observed, which arose from the complicated C and D transitions.[48,49] In agreement with the UV-vis spectrum, a strong room temperature photoluminence spectrum was recorded at 1.98 eV (Fig. 4d), corresponding to the band gap emission, which has previously been reported within monolayer regions.[20,21] In contrast, the band-gap photoluminescence of bulk MoS_2 was negligible because of its indirect bandgap nature.

3.2 Growth mechanism of MoS_2 monolayer

The growth process of MoS_2 monolayers was explored by carrying out the experiments as follows: (1) We synthesized the MoS_2 films on an unannealed Mo foil and observed the presence of thick films with lots of holes on 285 nm SiO_2/Si, which resulted from a large number of nucleation sites including scratches and rough edges from special pretreatment (Fig. S4, ESI†). Evidently, the high-temperature pre-annealing was employed to enlarge the Mo grains as well as to improve overall sample cleanliness, which was similar to the pretreatment on the graphene growth.[50] (2) We investigated the influence of the amount of sulfur powders on the quality of as-prepared MoS_2 atomic layers (Fig. S5, ESI†). The sulfur vapor can play two roles: reacting with the Mo foil to form MoS_2, and reacting with residual oxygen atoms to exclude impurities in our system. When 0.2 gram sulfur powders were used, the monolayer MoS_2 was still formed but the film has weak crystallinity (Fig. S5a, ESI†). When the amount of sulfur powers was increased to 1 gram, excessive sulfur clusters overburdened the Mo foil surface, which resulted in thick MoS_2 films (Fig. S5b, ESI†). (3) The influence of reaction time and temperature on the quality of MoS_2 films was studied in detail. As the reaction undergoing at 600 ^oC, we found that thick films were formed when the duration was over 10 min (Fig. 5a), and the thicker films were produced when the reaction was allowed to proceed for 60 min (Fig. 5c), which were demonstrated by optical contrast and Raman spectroscopy (Fig. 5(d-f)).[46] The frequency difference of the two characteristic $E_{2g}{}^1$ and A_{1g} modes ranging from 21-24 cm^{-1} suggested that the thin films were around 2-4 layers.[46] When the reaction temperature was allowed to decrease to 500 ^oC, large-area and uniform monolayers were formed for over 60 min (Fig. S6, ESI†). Further decreasing the reaction temperature down to 400 ^oC, discontinuous thin films were only produced (Fig. S7a and b, ESI†). When the temperature was more than 700 ^oC for 1 min, thicker films was formed (Fig. S7c, ESI†), and discontinuous films were observed after further prolonging the duration over 10 min (Fig. S7d, ESI†). In sharp contrast with the monolayers, the observed rupture in the multilayer MoS_2 film was resulted from weak van der Waals force between the SiO_2/Si substrate and the film. Dependence of growth of the as-synthesized MoS_2 thin films on the reaction temperature and time was summarized in Fig. S8 (ESI†).

Nanoscale Accepted Manuscript

This journal is © The Royal Society of Chemistry 20xx

Please do not adjust margins

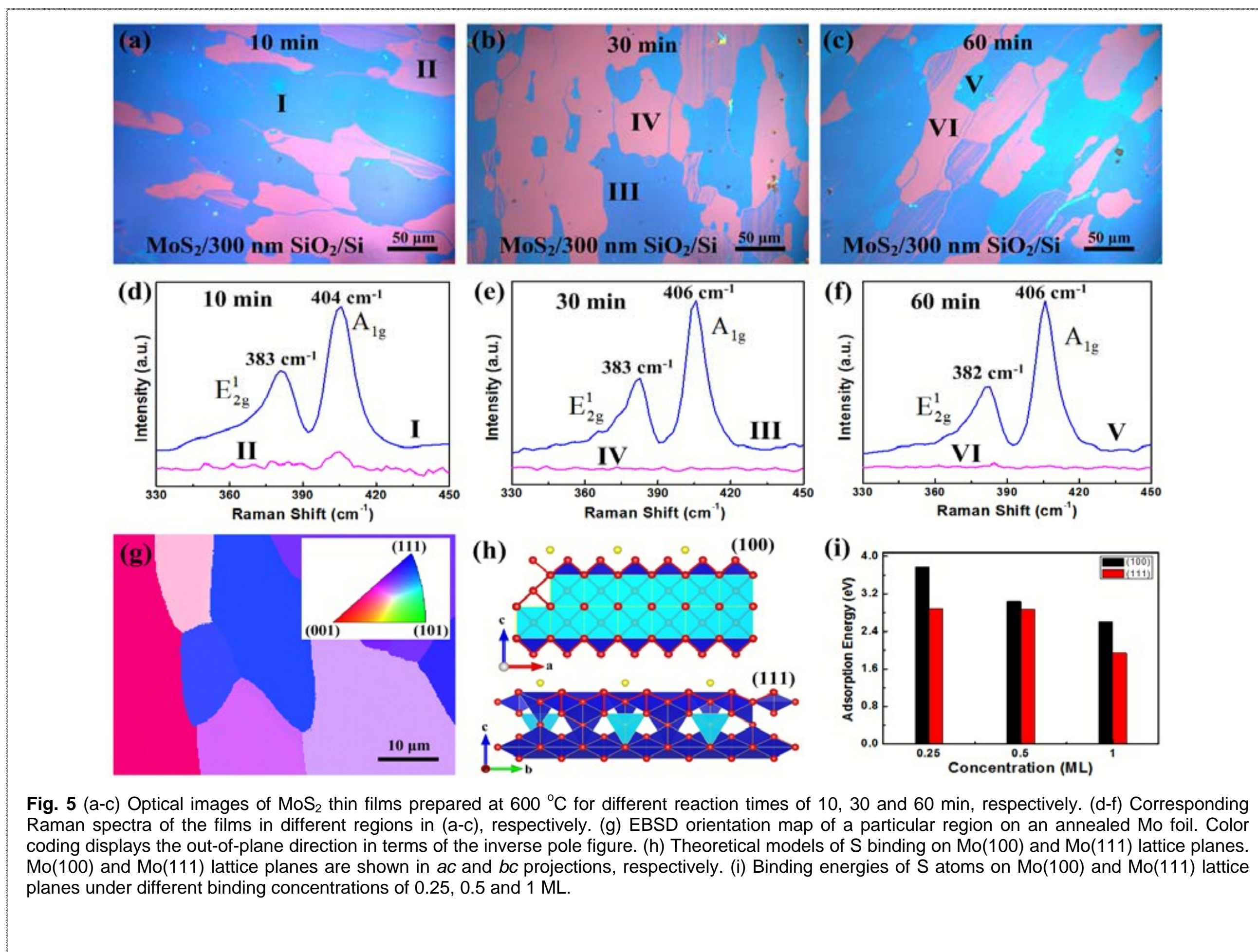

Fig. 5 (a-c) Optical images of MoS_2 thin films prepared at 600 ^oC for different reaction times of 10, 30 and 60 min, respectively. (d-f) Corresponding Raman spectra of the films in different regions in (a-c), respectively. (g) EBSD orientation map of a particular region on an annealed Mo foil. Color coding displays the out-of-plane direction in terms of the inverse pole figure. (h) Theoretical models of S binding on Mo(100) and Mo(111) lattice planes. Mo(100) and Mo(111) lattice planes are shown in *ac* and *bc* projections, respectively. (i) Binding energies of S atoms on Mo(100) and Mo(111) lattice planes under different binding concentrations of 0.25, 0.5 and 1 ML.

Based on the above investigations, we propose the following mechanism. The temperature determines the diffuse rate of S atoms on Mo foils. The controllable preparation of MoS_2 monolayers is directly dependent on the diffusion rate, which can be divided into surface and bulk diffusion rates. MoS_2 films grown at low temperature are thinner than those at high temperature, suggesting that the surface diffusion rate is higher than the bulk diffusion rate at low temperature. Generally, surface diffusion is orders of magnitude higher than the bulk and grain boundary diffusion.[51] According to the solid-state crystal growth theory, when the surface diffusion rate of S atoms on the Mo foil is higher than the bulk diffusion rate, the S atoms around the Mo foil surface will first precipitate, then reach super-saturation and finally react with the top layer of Mo atoms on the Mo foil. The dependence of thickness of the obtained MoS_2 films on the reaction temperature has been shown in Fig. S8.

We also observed that some regions in the thin films disappeared with prolonging the reaction duration over 10 min at 600 ^oC, while other regions still kept the similar thickness. In order to reveal the reasons, we visually imaged the structure of an annealed Mo foil by electron backscatter diffraction (EBSD) map (Fig. 5g). The EBSD map was captured to correlate the edge length and the crystallographic orientation of Mo grains. The map showed that the formed grain sizes were over 50 μm on the annealed Mo foil. Two Mo grains of Mo(100) and Mo(111) orientations were determined by the corresponding EBSD map in Fig. 5g, which was in good agreement with the corresponding XRD pattern of the annealed Mo foil (Fig. S1d, ESI†). In contrast, the orientations of the grains on an unannealed Mo foil were randomly distributed, and their sizes were mostly less than 5 μm (Fig. S9, ESI†). Although two kinds of lattice orientations, Mo(100) and Mo(111), were exactly verified by the EBSD map and the XRD pattern, we could still not discern what lattice plane is directed toward the thick films. We could also not distinguish what lattice plane was correlated with the disappearance of the films as the time progressed.

To elucidate the underlying mechanism of the observed facet-dependent growth of MoS_2 in our experiments, the binding energies of S atoms and Mo(100) as well as Mo(111) planes were calculated by first-principles calculations within density functional theory (DFT) framework. The most stable binding geometries of S atoms with different concentrations on Mo(100) and Mo(111) were shown in Fig. 5h (the detailed geometries was presented in Fig. S10 (ESI†)), and the corresponding data were made into a column chart in Fig. 5i. It is found that $E_{bind}(100)$ values are 3.799, 3.038 and 2.599 eV, corresponding to 0.25, 0.5 and 1 ML S clusters on Mo(100) surface, respectively, while $E_{bind}(111)$ values are 2.888, 2.875, 1.939 eV, respectively (Table S1). The results clearly show that binding energies of S atoms on Mo(100) are stronger than those on Mo(111). The binding energy difference can be reasonably adopted to explain the observed preferential growth of MoS_2 on Mo(100) facets at 600 ^oC. Based on the theoretical prediction for the binding and aggregation processes of the adatom on metal surfaces, the

Nanoscale Accepted Manuscript

growth of honeycomb-like materials is expected to be strongly dependent on the surface energy.[52,53] Because of high surface energy of Mo(100)-like surface, the S clusters can quickly adhere to the Mo(100)-like surface to reduce its energy, which leads to the fast nucleation and growth of the MoS_2 atomic layers.

Besides, MoS_2 thin films on Mo(111)-like surface disappeared as the time progressed due to low binding energy of S clusters on the surface, which resulted in weak bonding between the S clusters and Mo atoms on Mo(111). The disappearance of the thin films predominantly occurs through thermal sublimation process of the thin films.[54] It is noteworthy that a complete understanding of the MoS_2 growth process from theoretical calculations is still challenging. A thorough investigation of the atomistic mechanism for MoS_2 growth on Mo substrates would be a subject of future studies. However, regardless of the grain shapes and their binding energies, uniform MoS_2 monolayers can be prepared controllably at 600 °C within 1 min.

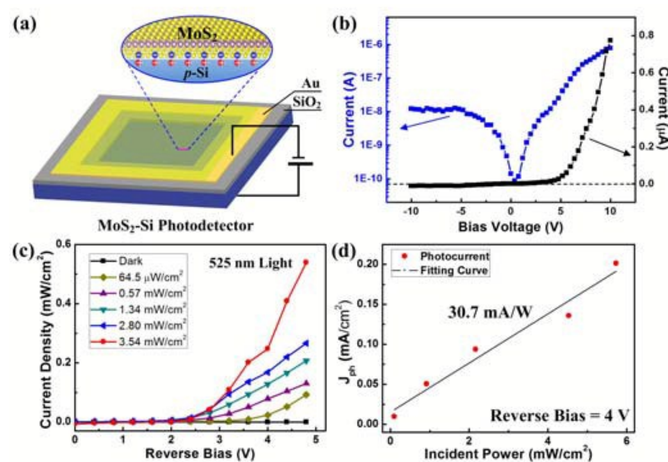

Fig. 6 (a) Schematic diagram of a vertical MoS_2-Si heterojunction device under light irradiation. A LED light with a wavelength of 525 nm was used. (b) Current-voltage (*I-V*) characteristic and corresponding logarithmic *I-V* curve of the device under darkness, showing a good rectifying behavior. (c) Total current densities as a function of external reverse biases under varying incident light powers. (d) Photocurrent response of the MoS_2-Silicon photodetector as a function of the incident light powers at a reverse bias of 4 V.

3.3 Photodetection properties of MoS_2-Si heterostructures

To evaluate the photodetection of the monolayer MoS_2, we fabricated a vertical heterojunction composed of monolayer MoS_2 and *p*-type silicon (*p*-Si), and corresponding schematic of the monolayer MoS_2/*p*-Si device was shown in Fig. 6a. Obvious rectifying behavior was observed and the rectifying ratio measured at ±10 V is up to 10^2 in dark because the band bending occurred at the monolayer MoS_2 and *p*-Si interface, which induced the presence of a built-in potential that promised an excellent photoresponse performance (Fig. 6b).[55-57] The photoresponse of the device was examined by exposing to a 525 nm light, as shown in Fig. 6c. The total current density (J_{total}) was plotted as a function of voltage in the device with an active area of 4 mm^2 under varying illumination powers, and the increase of short-circuit current (I_{sc}) was observed under illumination, indicating that light absorption in the n-MoS_2 and p-Si generated a photocurrent due to the production of electron-hole pairs. We found that the higher the reverse dc biases are, the larger the I_{sc} will be, which is due to the increased energy barrier height at the junction of the n-MoS_2 and the p-Si at a higher reverse bias. Furthermore, photoresponsivity of the device was calculated as the ratio of photocurrent to incident power at a reverse bias of 4 V, as shown in Fig. 6d. The photoresponsivity is up to 30.7 mA/W for an unoptimized device, which is remarkably higher than those of the first monolayer MoS_2 phototransistors (7.5 mA/W) and graphene-based devices (6.1 mA/W),[58,59] but lower than those of multilayer MoS_2 photodetectors.[56,57,60] We reasonably expect to further improve the performance of such hybrid photodetectors by doping and varying the film thickness.

4. Conclusions

In conclusion, we have developed an efficient method for large-area growth of MoS_2 monolayers by directly sulfurizing the Mo foils in sulfur vapor at 600 °C within 1 min. In sharp contrast to the growth of MoS_2 monolayers on insulating substrates, the obtained uniform monolayers can easily be transferred onto various substrates by removing the Mo foil using diluted $FeCl_3$ solution. Our work presents the effect of crystal orientation of Mo substrates on the synthesis of MoS_2 thin films and proposes a route of synthesizing large-domain and monolayer MoS_2. A p-n heterojunction device composed of monolayer MoS_2 and p-Si was fabricated to demonstrate its application in photodetectors. This study provides a new avenue for industrial scale applications of TMD thin films in future electronic and optoelectronic devices.

Acknowledgements

This work was supported by the NSF (61474063, 11302100, 51375240, 51472117 and 51535005), 973 program (2013CB932604 and 2012CB933403), Jiangsu NSF (SBK2015022205), the Innovation Fund of NUAA (NS2013095, NE2015102, NJ20140002, NJ20140003, NZ2015101 and NP2015203), SKL Funding of NUAA (0413Y02, 0415G02 and 0414K01), and the Priority Academic Program Development of Jiangsu Higher Education Institutions.

Notes and references

1 F. Bonaccorso, Z. Sun, T. Hasan and A. C. Ferrari, *Nat. Photonics,* 2010, **4**, 611–622.
2 K. S. Novoselov, V. I. Fal'ko, L. Colombo, P. R. Gellert, M. G. Schwab and K. Kim, *Nature*, 2012, **490**, 192–200.
3 F. N. Xia, H. Wang, D. Xiao, M. Dubey and A. Ramasubramaniam, *Nat. Photonics*, 2014, **8**, 899–907.
4 F. H. L. Koppens, T. Mueller, P. Avouris, A. C. Ferrari, M. S. Vitiello and M. Polini, *Nat. Nanotechnol.,* 2014, **9**, 780–793.
5 S. Das, J. A. Robinson, M. Dubey, H. Terrones and M. Terrones, *Ann. Rev. Mater. Res.,* 2015, **45**, 1–27.
6 G. Tai, T. S. Hu, Y. G. Zhou, X. F. Wang, J. Z. Kong, T. Zeng, Y. C. You and Q. Wang, *Angew. Chem. Int. Edit.*, 2015, DOI: 10.1002/anie.201509285.
7 S. L. Zhang, Z. Yan, Y. F. Li, Z. F. Chen and H. B. Zeng, *Angew. Chem. Int. Edit.*, 2015, **54**, 3112–3115.

Nanoscale Accepted Manuscript

This journal is © The Royal Society of Chemistry 20xx

Please do not adjust margins

8 H. Zhang, *ACS Nano*, 2015, **9**, 9451–9469.
9 H. Li, J. Wu, Z. Y. Yin and H. Zhang, *Acc. Chem. Res.*, 2014, **47**, 1067–1075.
10 X. Huang,Z. Zeng,Z. Fan, J. Liu and H. Zhang, *Adv. Mater.*, 2012, **24**, 5979–6004.
11 Q. H. Wang, K. Kalantar-Zadeh, A. Kis, J. N. Coleman and M. S. Strano, *Nat. Nanotechnol.,* 2012, **7**, 699–712.
12 L. Z. Kou, Y. D. Ma, X. Tan, T. Frauenheim, A. J. Du and S. Smith, *J. Phys. Chem. C,* 2015, **119**, 6918–6922.
13 O. V. Yazyev and Y. P. Chen, *Nat. Nanotechnol.,* 2014, **9**, 755–767.
14 S. Z. Butler, S. M. Hollen, L. Y. Cao, Y. Cui, J. A. Gupta, H. R. Gutierrez, T. F. Heinz, S. S. Hong, J. X. Huang, A. F. Ismach, E. Johnston-Halperin, M. Kuno, V. V. Plashnitsa, R. D. Robinson, R. S. Ruoff, S. Salahuddin, J. Shan, L. Shi, M. G. Spencer, M. Terrones, W. Windl and J. E. Goldberger, *ACS Nano,* 2013, **7**, 2898–2926.
15 R. Lv, J. A. Robinson, R. E. Schaak, D. Sun, Y. F. Sun, T. E. Mallouk and M. Terrones, *Accounts Chem. Res.,* 2015, **48**, 56–64.
16 M. Chhowalla, Z. F. Liu and H. Zhang, *Chem. Soc. Rev.,* 2015, **44**, 2584–2586.
17 C. Tan and H. Zhang, *Chem. Soc. Rev.*, 2015, **44**, 2713–2731.
18 X. Huang, Z. Zeng and H. Zhang, *Chem. Soc. Rev.*, 2013, **42**, 1934–1946.
19 X. Huang, C. Tan, Z. Yin and H. Zhang, *Adv. Mater.*, 2014, **26**, 2185–2204.
20 K. F. Mak, C. Lee, J. Hone, J. Shan and T. F. Heinz, *Phys. Rev. Lett.,* 2010, **105**, 136805.
21 S. H. Song, B. H. Kim, D. H. Choe, J. Kim, D. C. Kim, D. J. Lee, J. M. Kim, K. J. Chang and S. Jeon, *Adv. Mater.,* 2015, **27**, 3152–3158.
22 B. Radisavljevic, A. Radenovic, J. Brivio, V. Giacometti and A. Kis, *Nat. Nanotechnol.,* 2011, **6**, 147–150.
23 J. T. Ye, Y. J. Zhang, R. Akashi, M. S. Bahramy, R. Arita and Y. Iwasa, *Science,* 2012, **338**, 1193–1196.
24 A. Splendiani, L. Sun, Y. B. Zhang, T. S. Li, J. Kim, C. Y. Chim, G. Galli and F. Wang, *Nano Lett.,* 2010, **10**, 1271–1275.
25 B. Radisavljevic and A. Kis, *Nat. Mater.,* 2013, **12**, 815–820.
26 X. Cui, G.-H. Lee, Y. D. Kim, G. Arefe, P. Y. Huang, C.-H. Lee, D. A. Chenet, X. Zhang, L. Wang, F. Ye, F. Pizzocchero, B. S. Jessen, K. Watanabe, T. Taniguchi, D. A. Muller, T. Low, P. Kim and J. Hone, *Nat. Nanotechnol.,* 2015, **10**, 534–540.
27 B. Radisavljevic, M. B. Whitwick and A. Kis, *ACS Nano,* 2011, **5**, 9934–9938.
28 O. Lopez-Sanchez, D. Lembke, M. Kayci, A. Radenovic and A. Kis, *Nat. Nanotechnol.,* 2013, **8**, 497–501.
29 K. F. Mak, K. L. McGill, J. Park and P. L. McEuen, *Science,* 2014, **344**, 1489–1492.
30 K. K. Liu, W. J. Zhang, Y. H. Lee, Y. C. Lin, M. T. Chang, C. Su, C. S. Chang, H. Li, Y. M. Shi, H. Zhang, C. S. Lai and L. J. Li, *Nano Lett.,* 2012, **12**, 1538–1544.
31 Y. Lee, J. Lee, H. Bark, I.-K. Oh, G. H. Ryu, Z. Lee, H. Kim, J. H. Cho, J.-H. Ahn and C. Lee, *Nanoscale,* 2014, **6**, 2821–2826.
32 C. M. Orofeo, S. Suzuki, Y. Sekine and H. Hibino, *Appl. Phys. Lett.,* 2014, **105**, 083112.
33 Y. Zhan, Z. Liu, S. Najmaei, P. M. Ajayan and J. Lou, *Small,* 2012, **8**, 966–971.
34 Y. H. Lee, X. Q. Zhang, W. J. Zhang, M. T. Chang, C. T. Lin, K. D. Chang, Y. C. Yu, J. T. W. Wang, C. S. Chang, L. J. Li and T. W. Lin, *Adv. Mater.,* 2012, **24**, 2320–2325.
35 S. Najmaei, Z. Liu, W. Zhou, X. Zou, G. Shi, S. Lei, B. I. Yakobson, J.-C. Idrobo, P. M. Ajayan and J. Lou, *Nat. Mater.,* 2013, **12**, 754–759.
36 A. M. van der Zande, P. Y. Huang, D. A. Chenet, T. C. Berkelbach, Y. M. You, G. H. Lee, T. F. Heinz, D. R. Reichman, D. A. Muller and J. C. Hone, *Nat. Mater.,* 2013, **12**, 554–561.
37 K. Kang, S. E. Xie, L. J. Huang, Y. M. Han, P. Y. Huang, K. F. Mak, C. J. Kim, D. Muller and J. Park, *Nature,* 2015, **520**, 656–660.
38 Y. F. Yu, C. Li, Y. Liu, L. Q. Su, Y. Zhang and L. Y. Cao, *Sci. Rep.,* 2013, **3**, 1866.
39 Y. C. Lin, W. J. Zhang, J. K. Huang, K. K. Liu, Y. H. Lee, C. T. Liang, C. W. Chu and L. J. Li, *Nanoscale,* 2012, **4**, 6637–6641.
40 Q. Ji, Y. Zhang, T. Gao, Y. Zhang, D. Ma, M. Liu, Y. Chen, X. Qiao, P.-H. Tan, M. Kan, J. Feng, Q. Sun and Z. Liu, *Nano Lett.,* 2013, **13**, 3870–3877.
41 Y. M. Shi, W. Zhou, A. Y. Lu, W. J. Fang, Y. H. Lee, A. L. Hsu, S. M. Kim, K. K. Kim, H. Y. Yang, L. J. Li, J. C. Idrobo and J. Kong, *Nano Lett.,* 2012, **12**, 2784–2791.
42 I. Popov, G. Seifert and D. Tomanek, *Phys. Rev. Lett.,* 2012, **108**, 156802
43 H. L. Yu, C. Ma, B. H. Ge, Y. J. Chen, Z. Xu, C. L. Zhu, C. Y. Li, Q. Y. Ouyang, P. Gao, J. Q. Li, C. W. Sun, L. H. Qi, Y. M. Wang and F. H. Li, *Chem-Eur. J.,* 2013, **19**, 5818–5823.
44 G. L. Frey, R. Tenne, M. J. Matthews, M. S. Dresselhaus and G. Dresselhaus, *Phys. Rev. B,* 1999, **60**, 2883.
45 H. L. Zeng, B. R. Zhu, K. Liu, J. H. Fan, X. D. Cui and Q. M. Zhang, *Phys. Rev. B,* 2012, **86**, 241301.
46 H. Li, Q. Zhang, C. C. R. Yap, B. K. Tay, T. H. T. Edwin, A. Olivier and D. Baillargeat, *Adv. Funct. Mater.,* 2012, **22**, 1385–1390.
47 K. F. Mak, K. L. He, C. Lee, G. H. Lee, J. Hone, T. F. Heinz and J. Shan, *Nat. Mater.,* 2013, **12**, 207–211.
48 G. Eda, H. Yamaguchi, D. Voiry, T. Fujita, M. W. Chen and M. Chhowalla, *Nano Lett.,* 2011, **11**, 5111–5116.
49 E. M. Mannebach, K. A. N. Duerloo, L. A. Pellouchoud, M. J. Sher, S. Nah, Y. H. Kuo, Y. F. Yu, A. F. Marshall, L. Y. Cao, E. J. Reed and A. M. Lindenberg, *ACS Nano,* 2014, **8**, 10734–10742.
50 G. Tai, K. Wang, Z. Sun, J. Yin, S. M. Ng, J. Zhou, F. Yan, C. W. Leung, K. H. Wong, W. Guo and S. P. Lau, *J. Phys. Chem. C,* 2012, **116**, 532–537.
51 G. Antczak, G. Ehrlich, *Surface Diffusion: Metals, Metal Atoms, and Clusters*, Cambridge University Press, Cambridge, UK, **2010**.
52 R. T. Vang, K. Honkala, S. Dahl, E. K. Vestergaard, J. Schnadt, E. Laegsgaard, B. S. Clausen, J. K. Norskov and F. Besenbacher, *Nat. Mater.,* 2005, **4**, 160–162.
53 H. Chen, W. G. Zhu and Z. Y. Zhang, *Phys. Rev. Lett.,* 2010, **104**, 186101.
54 Y. K. Huang, J. D. Cain, L. Peng, S. Q. Hao, T. Chasapis, M. G. Kanatzidis, C. Wolverton, M. Grayson and V. P. Dravid, *ACS Nano,* 2014, **8**, 10851–10857.
55 M. L. Tsai, S. H. Su, J. K. Chang, D. S. Tsai, C. H. Chen, C. I. Wu, L. J. Li, L. J. Chen and J. H. He, *ACS Nano,* 2014, **8**, 8317–8322.
56 C. Yim, M. O'Brien, N. McEvoy, S. Riazimehr, H. Schafer-Eberwein, A. Bablich, R. Pawar, G. Iannaccone, C. Downing, G. Fiori, M. C. Lemme and G. S. Duesberg, *Sci. Rep.,* 2014, **4**, 5458.
57 M. R. Esmaeili-Rad and S. Salahuddin, *Sci Rep.,* 2013, **3**, 2345.
58 Z. Y. Yin, H. Li, H. Li, L. Jiang, Y. M. Shi, Y. H. Sun, G. Lu, Q. Zhang, X. D. Chen and H. Zhang, *ACS Nano,* 2012, **6**, 74–80.
59 T. Mueller, F. N. A. Xia and P. Avouris, *Nat. Photonics,* 2010, **4**, 297–301.
60 W. Choi, M. Y. Cho, A. Konar, J. H. Lee, G. B. Cha, S. C. Hong, S. Kim, J. Kim, D. Jena, J. Joo and S. Kim, *Adv. Mater.,* 2012, **24**, 5832–5836.

Nanoscale Accepted Manuscript

This journal is © The Royal Society of Chemistry 20xx

Please do not adjust margins